

Simulated laser-pulse evolution for high-order harmonic generation in a semi-infinite gas cell

Matthew Turner, Nicole Brimhall, Michael Ware, and Justin Peatross*

Department of Physics and Astronomy, Brigham Young University, Provo, Utah 84602

*Corresponding author: peat@byu.edu

Abstract: We numerically simulate the propagation of high-intensity laser pulses in helium to investigate the role of nonlinear effects in gas-cell high-harmonics experiments. An aperture located before the focusing lens is also included in the simulation. Numerical results for the radial fluence profile as a function of axial position, as well as for the spectral shift and ionization levels, agree with experimental observations. The simulations confirm that a significant Kerr effect is not required to generate the observed double focus in the fluence. The beam simulation also permits an investigation of high-harmonic phase matching. Most of the harmonic energy is seen to come from the forward portion of the laser pulse, whereas the latter portion gives rise to the incidental double laser focusing. Good phase matching for the harmonics arises in large measure from a balance between the linear phase delay of the neutral atoms and the Gouy shift, which is elongated and nearly linearized when the aperture is partially closed on the beam.

© 2008 Optical Society of America

OCIS codes: (190.4160) multiharmonic generation; (190.5530) pulse propagation and temporal solitons; (190.5940) self-action effects; (190.7110) ultrafast nonlinear optics

References and links

1. J. C. Painter, M. Adams, N. Brimhall, E. Christensen, G. Giraud, N. Powers, M. Turner, M. Ware, and J. Peatross, "Direct observation of laser filamentation in high-order harmonic generation," *Opt. Lett.* **31**, 3471–3473 (2006).
2. N. Brimhall, J. C. Painter, N. Powers, G. Giraud, M. Turner, M. Ware, and J. Peatross, "Measured laser-beam evolution during high-order harmonic generation in a semi-infinite gas cell," *Opt. Express* **15**, 1684–1689 (2007).
3. V. Tosa and C. H. Nam, "Comment on 'Direct observation of laser filamentation in high-order harmonic generation'," *Opt. Lett.* **32**, 2707–2708 (2007).
4. M. Turner, N. Brimhall, M. Ware, and J. Peatross, "Reply to comment on 'Direct observation of laser filamentation in high-order harmonic generation'," *Opt. Lett.* **32**, 2709–2710 (2007).
5. A. Chiron, B. Lamouroux, R. Lange, J. F. Ripoche, M. Franco, B. Prade, G. Bonnaud, G. Riazuelo, and A. Mysyrowicz, "Numerical simulations of the nonlinear propagation of femtosecond optical pulses in gases," *Eur. Phys. J. D* **6**, 383–396 (1999).
6. S. Carusotto, E. Iacopini, E. Polacco, F. Scuri, G. Stefanini, and E. Zavattini, "Measurement of the Kerr constant of He, A, O₂, H₂, and D₂," *Nuovo Cimento* **5D**, 328–338 (1985).
7. M. Ammosov, N. Delone, and V. Krainov, "Tunnel ionization of complex atoms and of atomic ions in an alternating electromagnetic field," *Sov. Phys. JETP* **64**, 1191–1194 (1986).
8. S. L. Chin, S. A. Hosseini, W. Liu, Q. Luo, F. Theberge, N. Akozbek, A. Becker, V. P. Kandidov, O. G. Kosareva, and H. Schroeder, "The propagation of powerful femtosecond laser pulses in optical media: physics, applications, and new challenges," *Can. J. Phys.* **83**, 863–905 (2005).
9. H. T. Kim, I. J. Kim, V. Tosa, Y. S. Lee, and C. H. Nam, "High brightness harmonic generation at 13 nm using self-guided and chirped femtosecond laser pulses," *Appl. Phys. B* **78**, 863–867 (2004).

10. V. Tosa, E. Takahashi, Y. Nabekawa, and K. Midorikawa, "Generation of high-order harmonics in a self-guided beam," *Phys. Rev. A* **67**, 063817 (2003).
11. M. Lewenstein, P. Salieres, and A. L'Huillier, "Phase of the atomic polarization in high-order harmonic generation," *Phys. Rev. A* **62**, 4747–4754 (1995).
12. B. L. Henke, E. M. Gullikson, and J. C. Davis, *Atomic Data and Nuclear Tables*, vol. 54 (Academic, San Diego, 1993); see http://henke.lbl.gov/optical_constants/.
13. J. Sutherland, E. Christensen, N. Powers, S. Rhynard, P. Painter, and J. Peatross, "High harmonic generation in a semi-infinite gas cell," *Opt. Express* **12**, 4430–4436 (2004).
14. S. Kazamias, F. Weihe, D. Douillet, C. Valentin, T. Planchon, S. Sebban, G. Grillon, F. Augé, D. Hulin, and P. Balcou, "High order harmonic generation optimization with an apertured laser beam," *Eur. Phys. J. D* **21**, 353–359 (2002).

1. Introduction

We recently published experimental measurements of laser beam evolution in our high-harmonic generation setup [1, 2]. The measurements showed the beam fluence narrowing to two separate foci, separated by a distance of about 7 cm. This behavior occurs with peak pulse power an order of magnitude smaller than expected for Kerr self-focusing in our helium-filled cell. Tosa and Nam [3] pointed out that Kerr self-focusing is not necessary to explain the double focusing in our experimental arrangement, based on simulations of laser propagation. We independently came to the same conclusion [4] based on similar simulations. In this paper we present details and results of our simulations and examine the phase matching for the high harmonics in comparison with experiment. We find that good phase matching occurs for the front of the laser pulse but not the back where ionization and nonlinear effects take place. Because the phase matching varies within the pulse as it travels, it is helpful to view it dynamically in the form of a movie.

2. Simulation method and parameters

The experimental parameters of our laser pulse lend themselves to a number of computational approximations. We base our simulations on the method outlined by Chiron *et al.* [5], which uses the slowly-varying envelope and paraxial approximations to the scalar wave equation with radial symmetry and neglects group velocity dispersion. In a moving frame, this equation is given by

$$\frac{2ik_0c}{\omega_0} \frac{\partial E}{\partial \eta} + \nabla_\rho^2 E + 2n_0 \Delta n E = 0, \quad (1)$$

where E is the field envelope multiplying a plane wave oscillating at ω_0 . The wave number k_0 is evaluated in the neutral gas medium with index n_0 . The change in index due to the Kerr effect and plasma generation is described by $\Delta n \approx n_2 I - \omega_p^2 / 2\omega_0^2$, with $n_2 = 3.5 \times 10^{-21} \text{ cm}^2/\text{W}$ corresponding to an atmosphere of helium [6]. The plasma frequency ω_p , associated with free electrons, is determined using the ADK ionization model [7]. The variables $\eta = z/(c/\omega_0)$ and $\tau = \omega_0[t - \eta/(k_0c)]$ track the pulse in a moving frame, which reduces the computational load. Here t is time, z is the axial propagation distance, and ρ is the radial position. We treat Δn for a given point in the moving frame as approximately constant from one computed frame to the next, typically 250 microns apart. Smaller step sizes yield the same results to within 1% after 10 cm of propagation. We verified that our code recovers the analytical solution for a Gaussian pulse propagated in vacuum and that a Kerr-induced collapse occurs at the critical power [8] (when the pressure is set far above that of our experiments).

The parameters for the simulation are chosen to be similar to those of our experiments: the pulse is taken to have a Gaussian temporal profile with 35 fs FWHM and to have a center wavelength of 800 nm. (There is some uncertainty in the 30 fs reported for the experiments; the simulations done with 35 fs agrees better with the experimental results.) The spatial profile of

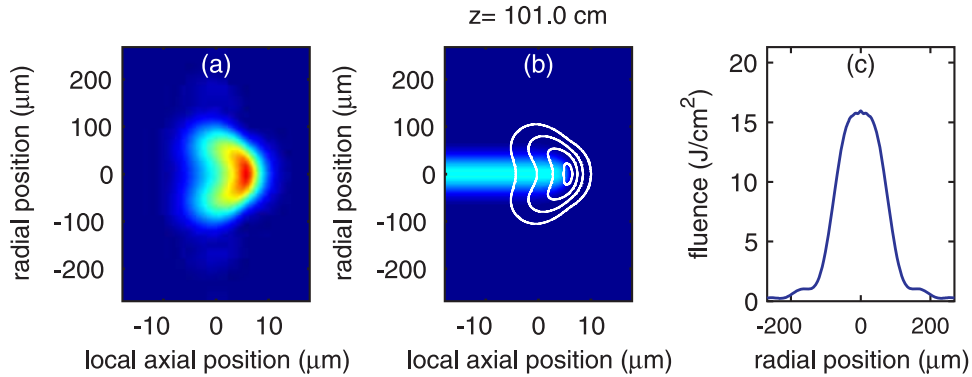


Fig. 1. Movie of the (a) pulse intensity (dark red indicates the peak intensity of 5.7×10^{14} W/cm²), (b) free-electron density (dark red indicates the peak free-electron density of 5.3×10^{22} electrons/m³, equivalent to 2.1% ionization), and (c) fluence as the pulse propagates 10 cm through the focus. Each frame shows a snapshot of the pulse at locations 1 mm apart along the direction of travel. The contour lines in frame (b) indicate pulse intensity, with lines representing a 20% change in intensity. (4.7 MB)

the laser is taken initially to be Gaussian with a $1/e^2$ diameter of 11 mm, and then clipped by a 9 mm aperture placed in the beam path. The pulse energy before the aperture is set to 6.84 mJ, which reduces in the simulation to 5 mJ after the aperture. The aperture is placed 145 cm before a concave mirror with 100 cm focal length. With the aperture in the beam, it focuses in vacuum to a peak intensity of 1.3×10^{15} W/cm². Fresnel diffraction integrals are used to calculate the initial pulse profile 5 cm before the nominal beam focus, taking into account the effects of the aperture and focusing mirror on the incoming pulse. A Crank-Nicolson algorithm is then used to propagate the pulse in the vicinity of the focus, where nonlinear effects become important.

3. Simulation results

The two left frames of Fig. 1 show movies of the pulse intensity and the free-electron density, respectively, as the pulse propagates 10 cm through the focus (i.e., from 95 cm to 105 cm after the focusing mirror). Each frame in the movie shows a snapshot of the pulse at locations 1 mm apart along the direction of travel. As seen in the movie, the early generation of plasma causes the back of the pulse to refract outward to form a ring. As described by Kim *et al.* [9], some beam energy at wider radii misses the plasma and continues to converge toward the axis downstream. This effect is enhanced for the apertured beam (which has an elongated focal region) and accounts for the dual focus when the gas is introduced. We find that the peak density of generated plasma represents about 2% ionization of the neutral medium. The combined ionization and pondermotive-excitation energies represent 3% of the available pulse energy, which we approximate as undepleted in the simulation. This is consistent with our experimental measurement, which showed that the energy lost in the interaction was less than 10% (an upper limit set by the uncertainty in our energy measurement).

Experimentally, we previously measured fluence profiles of our pulse in the region of the focus [1, 2]. To compare with the data in those reports, Fig. 1(c) shows a line-out of the time-integrated intensity, or fluence in units of energy per area from the simulation. These radial fluence profiles exhibit several key features in agreement with experimental data, including the occurrence of a flat-top profile noted by Tosa *et al.* [10]. The simulations reveal that the flat-top profile arises from a combination of the undistorted front of the pulse and the ring structure at

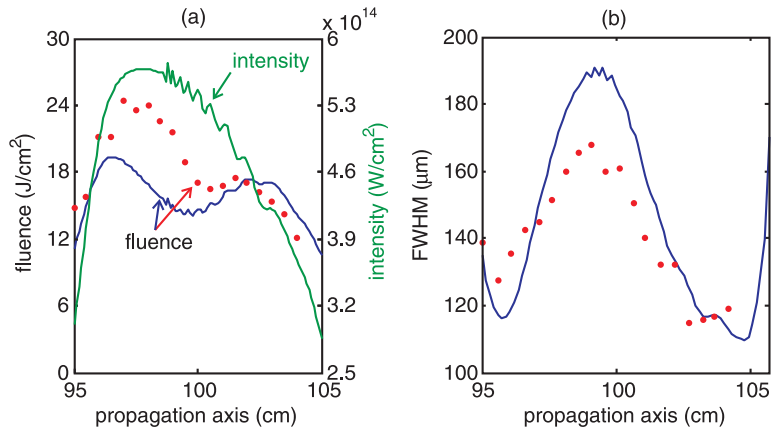


Fig. 2. (a) The on-axis fluence from the experiment (dots) and simulation (line), and the calculated peak pulse intensity as a function of axial position in the focus. (b) FWHM values for the fluence along the propagation axis given by simulation (line) and by experiment (dots). The propagation axis location is given as a distance from the focusing optic ($f = 100$ cm).

the back of the pulse. As some of the outer energy continues to converge downstream where the intensity and plasma generation is less, there is a modest axial resurgence of fluence, giving rise to the second focus. This effect is enhanced by the unique focal geometry of the apertured beam; although it is present for a Gaussian beam, it is insufficient to produce a second focus.

Figure 2(a) shows the peak pulse intensity and the on-axis fluence as a function of axial position in the focus. Our previous experimental fluence measurements are also shown for comparison. As is evident, the peak intensity continuously decreases after an initial maximum. In contrast, the fluence undergoes a second local maximum. This implies an increased pulse duration at that location. Figure 2(b) shows the full-width-at-half-maximum of the fluence as the pulse propagates in the simulation. Note that the simulation reproduces the experimentally observed double focus profile [3,4]. Importantly, the dual focus arises without the need for Kerr-style filamentation that we previously suggested. This dismissal of a substantial Kerr effect is consistent with the fact that the peak power is an order of magnitude below the critical level for self-focusing. In fact, including or not including the Kerr effect at the accepted value [6] has almost no impact on the simulation. In contrast, if plasma generation is switched off in the simulation, the pulse propagation is virtually identical to that in vacuum.

The spectral blueshift of the simulated pulse at the nominal focus is 6 nm, which is in reasonable agreement with the experimentally observed blueshift of 4 nm. The overall agreement between the simulations and the experimental measurements lends confidence that the simulation code captures the essential physics of the pulse-medium interaction. The simulations can therefore be employed with reasonable confidence to investigate dynamic phase matching of high harmonics in our setup.

4. Phase matching

Phase mismatches in the high-harmonics generating process come from two sources: 1) conventional phase mismatches, which arise from the Gouy phase shift and the refractive index of the neutral atoms and generated plasma; 2) intrinsic phase mismatches, which arise from variations in the laser intensity. For harmonics in the plateau, the intrinsic intensity-dependent phase is expected to follow $\phi_{\text{int}} = -\pi I / 2.5 \times 10^{13} \text{ W/cm}^2$ for our laser frequency [11] (based

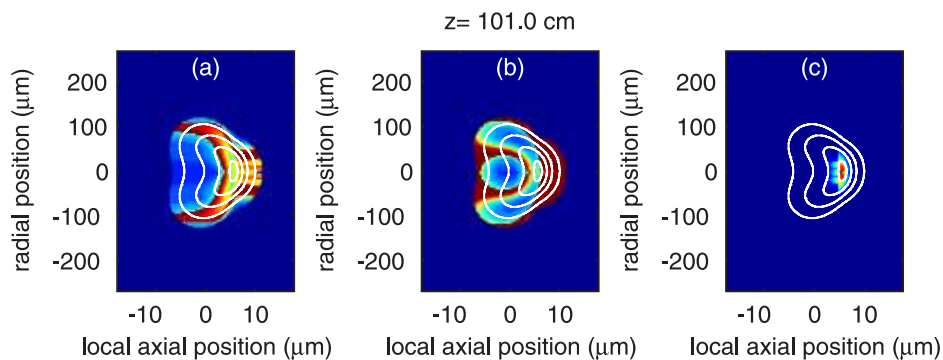


Fig. 3. Movie of coherence lengths of the 75th harmonic for each point on the pulse for (a) conventional and (b) intrinsic intensity-dependent phase. Coherence lengths have been capped at a reabsorption limit of 2 cm (dark red). (c) Movie of the fifth power of the laser intensity multiplied by the square of the coherence length (including both conventional and intrinsic phases) at each point on the pulse. The white contour lines indicate laser intensity. The dark red color in (c) indicates strong harmonic generation in arbitrary units. (4.2 MB)

on $\phi_{\text{int}} = -5.8U_p$, where $U_p = 1$ in atomic units corresponds to a ponderomotive potential of 27 eV). This can easily produce phase errors greater than π if the intensity of a given point on the traveling laser pulse varies by more than a few percent as the pulse propagates. Figures 3(a) and (b) show the forward-directed coherence lengths for each point on the pulse, based separately on the conventional and the intrinsic intensity-dependent phase mismatches, respectively. The coherence lengths, which are for the 75th harmonic, are computed by comparing the phase at a particular point in a frame with the phase of the corresponding points in past frames to find the maximum distance wherein the harmonic phase varies less than π . The coherence lengths were capped in the calculations at an estimated reabsorption limit of 2 cm [12].

The coherence length for the conventional phase shown in Fig. 3(a) is many millimeters long near the regions of high intensity. This good phase matching stems primarily from a fortuitous cancelation between the phase due to the linear index and the Gouy shift. (The index for the fundamental in 80 torr helium is $1 + 3.8 \times 10^{-6}$, whereas it is $1 - 2.7 \times 10^{-7}$ for the 75th harmonic. [12]) The aperture has the effect of linearizing the Gouy shift with axial position in the focus. This linearized Gouy shift, together with the phase error arising from a limited amount of plasma, tends to cancel with the linear dispersion of the neutral gas. In the case of decreasing intensity with z , the intrinsic phase mismatch shown in Fig. 3(b) introduces a phase slip with the same sign as that arising from the neutral gas.

The energy of harmonic emission depends nonlinearly on the laser intensity, which we approximate with a fifth-order power law (although a third-order power law, for example, gives qualitatively similar results). Efficient high-harmonic generation requires both high-intensity and good phase matching. Figure 3(c) shows the fifth power of the laser intensity multiplied by the square of the coherence length, computed with the combined conventional and intrinsic phases (not shown). In each frame, one can see the portions of the pulse that contribute to overall harmonic emission, assuming the harmonics exit into vacuum following the frame and continue on to a detector (as was done in the experiment by scanning the exit foil to different axial positions). The best overall phase matching occurs near $z = 101$ cm, where the separate phase mismatches indicated in Figs. 3(a) and (b) have similar magnitudes and opposite signs. Near the front of the pulse, the coherence length exceeds the reabsorption limit of 2 cm, in agreement with earlier direct experimental observation. On the other hand, as plasma is generated on the rear of the pulse, that portion of the pulse experiences poor phase matching.

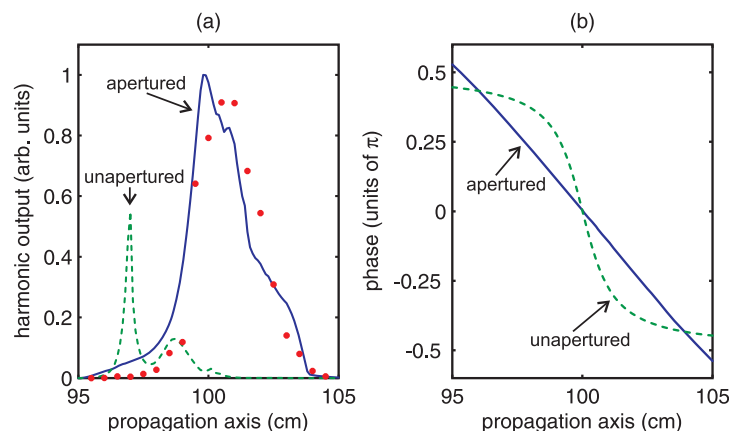


Fig. 4. (a) The calculated (solid line) and measured (dots) overall emission for the 75th harmonic with an aperture in the beam. Also plotted is calculated overall emission for the same harmonic with an unapertured pulse (dashed line). (b) Beam phase due to the Gouy shift for an apertured (solid line) and an unapertured (dashed line) beam.

By integrating each snapshot in Fig. 3(c) radially and longitudinally, the total harmonic energy emerging from each longitudinal step can be calculated. Figure 4(a) shows the calculated overall emission for the 75th harmonic at each longitudinal step. Our experimental results for the same harmonic are also shown for comparison. We find that the vast majority of the harmonic output comes from the forward part of the pulse, before significant ionization. The result is hardly affected if we exclude regions wherein ionization exceeds 10% of the peak amount.

We have observed experimentally that opening the aperture located before the focusing lens decreased the harmonic output by about an order of magnitude [13]. Our simulation also shows this dramatic behavior, which is plotted in Fig. 4(a). Since the simulation uses a smooth input beam, the aperture effect does not arise merely from spatially cleaning the laser beam. Rather, it is due primarily to linearizing the rate of the Gouy phase slip in the apertured case, as seen in Fig. 4(b). This is consistent with the analysis by Kazamias *et al.* [14] on the aperture effect.

5. Conclusion

Simulations demonstrate that the interplay between the focusing geometry of the apertured beam combined with refraction from plasma generation is responsible for the double focus observed in our experiments. Kerr-style self-focusing does not appear to play a role. The agreement between the simulations and the various experimental measurements lends credibility to using the simulations to assess phase-matching of high-order harmonics. The simulations suggest that the high harmonics produced in our helium-filled cell comes almost entirely from the forward, undistorted portion of the laser pulse. Harmonics are suppressed in the rear portion of the pulse that undergoes significant ionization. Thus, the self-guiding of the pulse and the occurrence of the second focus in fluence are only incidental in the sense that they arise from a part of the pulse that does not contribute to the high-harmonic output. The good phase matching we have observed experimentally arises in large part from the balancing of the linear index against the the Gouy shift, which varies almost linearly in z when an aperture is partially closed on the pre-focused beam. The intrinsic phase mismatch and that arising from a modest amount of plasma also participate in minimizing the phase mismatch.

This work is supported by NSF Grant PHY-0457316.